Evaluation of Different Soil Salinity Mapping Using Remote Sensing Indicators and Regression Techniques, Basrah, Iraq

Amal Muhammad Saleh

College of Agriculture / University of Baghdad
mhmmd1961@aol.com

Abstract: Soil salinity is one of the most damaging environmental problems especially in arid and semi-arid regions. Remotely sensed data with a significant correlation to ECe were considered for developing the regression models. The aim of this study was to develop statistical regression models based on remotely sensed data to predict and map spatial variation in soil salinity in Basrah area. Different spectral indices were calculated from original bands of Landsat OLI and TIRS satellite images. Statistical correlation between field measurements of Electrical Conductivity (ECe) with the salinity indices showed that the Brightness Index (BI_1) had the highest correlation with ECe ($R2 = 0.95$). Ordinary Cokriging geostatistical technique was applied to estimate and identify the spatial variability of ECe (the primary variable) with the soil salinity indices (the secondary variables). The results suggest that estimation can be significantly improved using Cokriging. Compared with the Ordinary Kriging results using only primary data set of ECe, Cokriging improves the estimations greatly by increasing correlation of estimated and actual ECe ($R2 = 0.668$). Soil salinity map generated by the Ordinary Cokriging procedure showed that strongly saline soils (>16 dS m-1) with variable spatial distribution were the dominant class over the study area. The results of these models allow to interpolate and classify salinity on a more realistic, and continuous scale.

1. Introduction

Soil salinity is a dynamic process with severe consequences for the soil, hydrological, climatic, geochemical, agricultural, social, and economic aspects. Information on the spatial extent, nature and distribution of soil salinity is becoming very essential. Thus, timely detection of soil salinity, monitoring and assessment of its severity level and extent become very important in its beginning at local and regional scales. (Allbed and Kumar, 2013). Soil salinity is a common form of land degradation in irrigated areas located in dry land environments. The physical appearance of salinity is strongly influenced by soil properties (e.g., moisture, texture, mineral composition, and surface roughness) as well as type of vegetation cover (e.g., halophyte and nonhalophyte, salt-tolerant and nonsalt-tolerant) (Farifteh et al., 2006).

Conventionally, soil salinity has been measured by collecting in situ soil samples and analyzing those samples in the laboratory to determine their solute concentrations or electrical conductivity. However, these methods are time-consuming and costly since dense sampling is required to adequately characterize the spatial variability of an area but remote sensing data and techniques offer more efficiently and economically rapid tools and techniques for monitoring and mapping soil salinity (Ghabour and Daels, 1993).

Remote sensing data and techniques have been progressively applied to monitor and map soil salinity since 1960s when black-and-white and color aerial photographs are used to delineate salt-affected soils (Dale et al., 1986). Satellite data has a great potential for monitoring salinization in both spatial and temporal extents. Remote sensing data can be used as input into a geographic information system (GIS) for further analysis and comparison to other data. Sensors with improved resolution are able to recognize more details for better results and precision. Using remote sensing, soil salinity can be mapped both directly, by reflectance from bare soil, or from the salt crust, and indirectly from vegetative coverage and health (Abbas and Khan, 2007).

The main objectives of this study are: (i) to develop effective combined spectral-based statistical regression models using Landsat OLI and TIRS satellite images, (ii) to predict and map spatial variation in soil salinity in a part of lower Mesopotamia of Iraq, Basrah area, using geostatistical techniques, integrating a limited data set of soil salinity measurements (ECe) as a primary variable with Landsat OLI and TIRS satellite image as a secondary data source. The result of this methodology will be qualified using the cross validation method.

2. Material and Methods

Basra is located on the Shatt-Al-Arab waterway, downstream of which is the Arabian Gulf. It is geographically situated on latitude 29º07'58.74"-31º17'15.88" North and longitude 46º34'19.63"-48º36'59.06" East (Fig. 1). Basra has a hot desert climate (Köppen climate classification BWh), like the rest of the surrounding region, though it receives slightly more precipitation than inland locations due to its location near the coast. During the summer months, Basra is consistently one of the hottest cities on the planet, with temperatures regularly exceeding 50 °C (122 °F) in July and August. In winter Basra experiences mild weather with average high temperatures around 20 °C (68 °F). High humidity-sometimes exceeding 90% - is common due to the proximity to the marshy Arabian Gulf. The rain is irregular and falls only during winter, the average annual precipitation in Basrah area is about 140 mm, and evaporation from 50 to 250/600 mm a month (January and July means). The ground water flow in Lower Mesopotamia basin is toward southeast i.e. toward Arabian Gulf., this water exhibit a seasonal and spatial variation according to geological, hydrological and environmental impact. The low level of Basrah surface and the availability of much surface water such as Arabian Gulf, Marshes, Shatt Al-Basrah, and Shatt Al-Arab River and its tributaries causing the high water table level, which increases the soil salinity under high evaporation rate (Al-Marsoumi and Al-Jabbri, 2007).

Based on the fieldwork and ground truth data performed by Ministry of Water Resources/National Center for Water Resources Management, A total number of 109 random soil profiles were examined in different locations. The exact coordinates of each soil profile were precisely defined in the field by a global positioning system (GPS). Fig. (2) shows the location of the observation sites where soil samples were collected from the surface horizon (0–20 cm). Electrical conductivity soil salinity measurements (ECe) dS m-1 were determined in the soil water extract out of the saturated soil paste (Page et al., 1982).

Soils were classified as Entisols according to Soil Taxonomy (Soil Survey Staff, 2014) (Table 1). In the Entisols, only Ochric epipedon existence was identified. All soil profiles are still in developing phase. Over all the soils are very high CaCO3 contents, but very low in organic matter.

The Landsat Operational Land Imager (OLI-8) satellite images were used in this study and were acquired near the actual soil sampling dates (Table 2). The images were georectified to a Universal Transverse Mercator (UTM) coordinate system, using World Geodetic System (WGS) 1984 datum, assigned, to north UTM zone 38-39. Typical atmospheric and radiometric corrections and spatial resolution enhancement were performed. All the remote sensing data processing was performed using ERDAS IMAGINE version 9.2 software.

Soil salinity detection using remote sensing techniques developed in numerous studies. In this study, we applied different indices for all the Landsat images to detect salt mineral in soils based on the different responses of salty soils to various spectral bands (Table 3). we removed panchromatic, cirrus, coastal aerosol, SWIR 1, SWIR 2 infrared, and thermal infrared bands. In addition to salinity indices, we used the bands B2, B3, B4, and B5 (centered respectively at 480, 560, 655, and 865 nm) to analyze the performances of Landsat spectral bands in detecting and mapping soil salinity.

Data were analysed statistically. Classical descriptors were determined, such as mean, maximum, minimum, standard deviation and skewness of data distribution. The Shapiro–Wilk statistic (W) was computed for ECe data set to test the normality of the distributions (Shapiro and Wilk, 1965).

Stepwise regression was used to determine the variables that best explained most of the variability of the dependent variable, which was ECe. All the developed regression models were tested, models with a high R^2 signifying a strongly linear relationship. The best performed regression model was chosen and used to predict and map the spatial variation in soil salinity. All statistical analyses were performed by IBM® SPSS® Statistics v.23.0 Software.

The variability of soil salinity representing horizontal distribution of salts in continuous model was mapped. Isotropic semivariogram and cross-semivariogram functions were calculated to quantify and model the spatial variability degree of ECe data (Isaaks and Srivastava, 1989). The experimental semivariogram for a regionalized variable of Z can be defined as follows:

$$\gamma(h) = \frac{1}{2N(h)} \sum_{i=1}^{N(h)} [z(x_i + h) - z(x_i)]^2 \quad (1)$$

where $\gamma(h)$ is the experimental semivariogram value at distance interval h; $N(h)$ is number of sample value pairs within the distance interval h; $z(x_i)$, $z(x_i + h)$ is sample values at two points separated by the distance interval h. R^2 was used to select the exact form and best fit of the semivariogram model. The spherical model defined in equation (2) provided the best fit for the experimental semivariance for original and de-trended data of ECe.
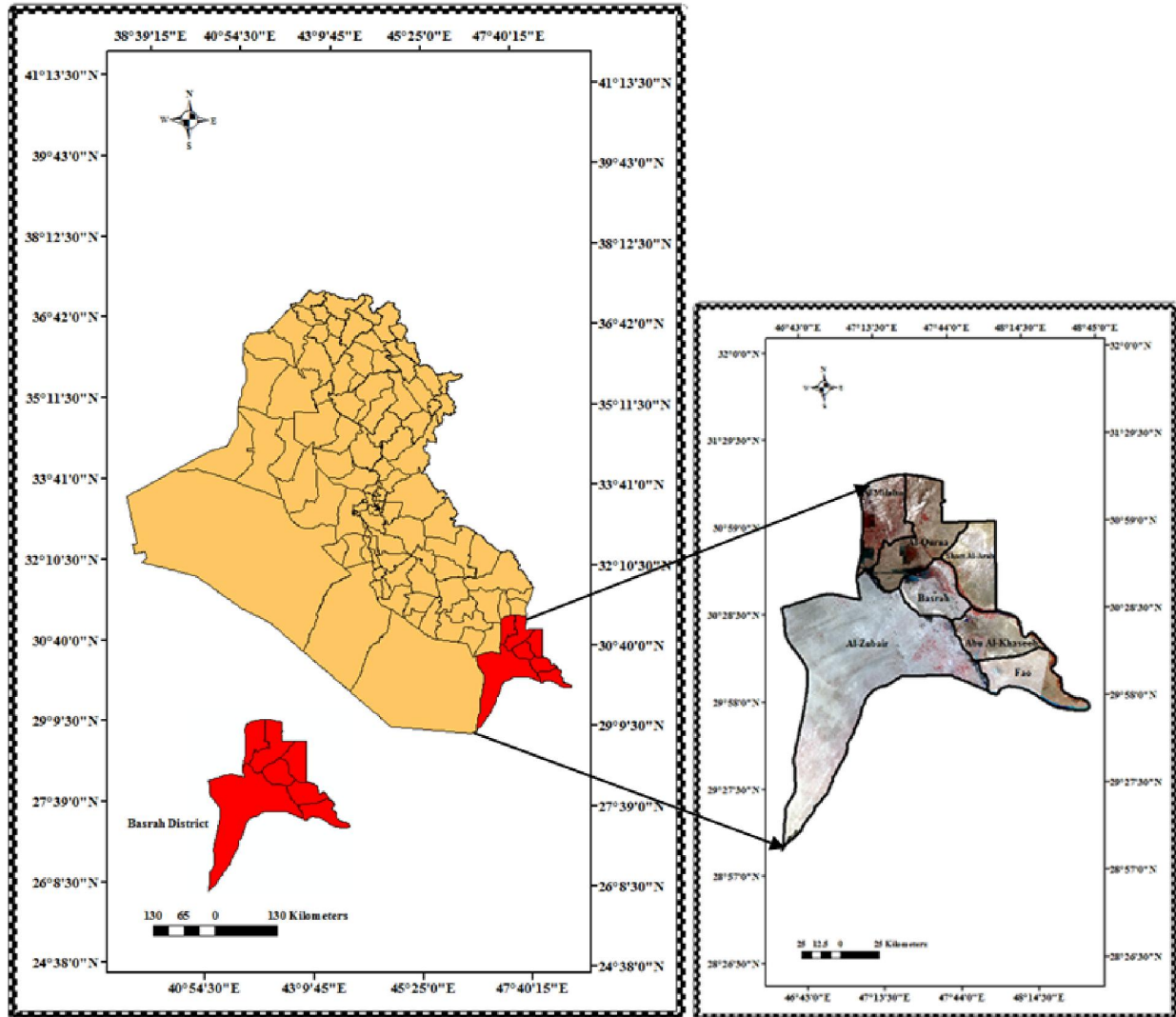
Figure 1. Location map of the study area.

Table 1. The classification of the soils according to Soil Taxonomy (Soil Survey Staff, 2014)

Order	Suborder	Great Group	Subgroup
Entisols	Fluvents	Torrifluvents	Typic Torrifluvents
	Pasmments	Torripasmments	Typic Torripasmments
Aridisols	Salids	Haplosalids	Typic Haplosalids

Table 2. The dates of field measurements and Landsat 8 acquisitions

Spacecraft_ID	Sensor_ID	No. of Bands	Resolution (m)	Path/ Row	Date_Acquired	Date of Field Measurements
Landsat_8	OLI_TIRS	Reflective (8)	30.00	165/038	2017-03-26	2017-03-10
				165/039	2017-03-26	2017-03-16
		Thermal (2)	30.00	165/040	2017-03-26	2017-03-20
				166/038	2017-04-02	2017-03-23
		Panchromatic (1)	15.00	166/039	2017-04-02	2017-03-27
				166/040	2017-04-02	2017-03-30

Table 3. The most common salinity indices used in this study

Salinity indices	Equation	Reference
Brightness index-1	$BI = \sqrt{(R^2 + NIR^2)}$	(Khan et al., 2005)
Brightness index-2	$BI = \sqrt{G^2 + NIR^2}$	(Fourati et al., 2015)
Salinity index-1	$SI = \sqrt{(B * R)}$	(Khan et al., 2001)
Salinity index-2	$SI = \sqrt{(G * R)}$	(Douaoui, 2006)
Salinity index-3	$SI = \sqrt{(G^2 + R^2)}$	(Douaoui, 2006)
Salinity index-4	$SI = \sqrt{(G^2 + R^2 + NIR^2)}$	(Douaoui, 2006)
Salinity index-5	$SI = G * R$	The proposed salinity index
Salinity index-6	$SI = \sqrt{G^2 * NIR^2}$	The proposed salinity index
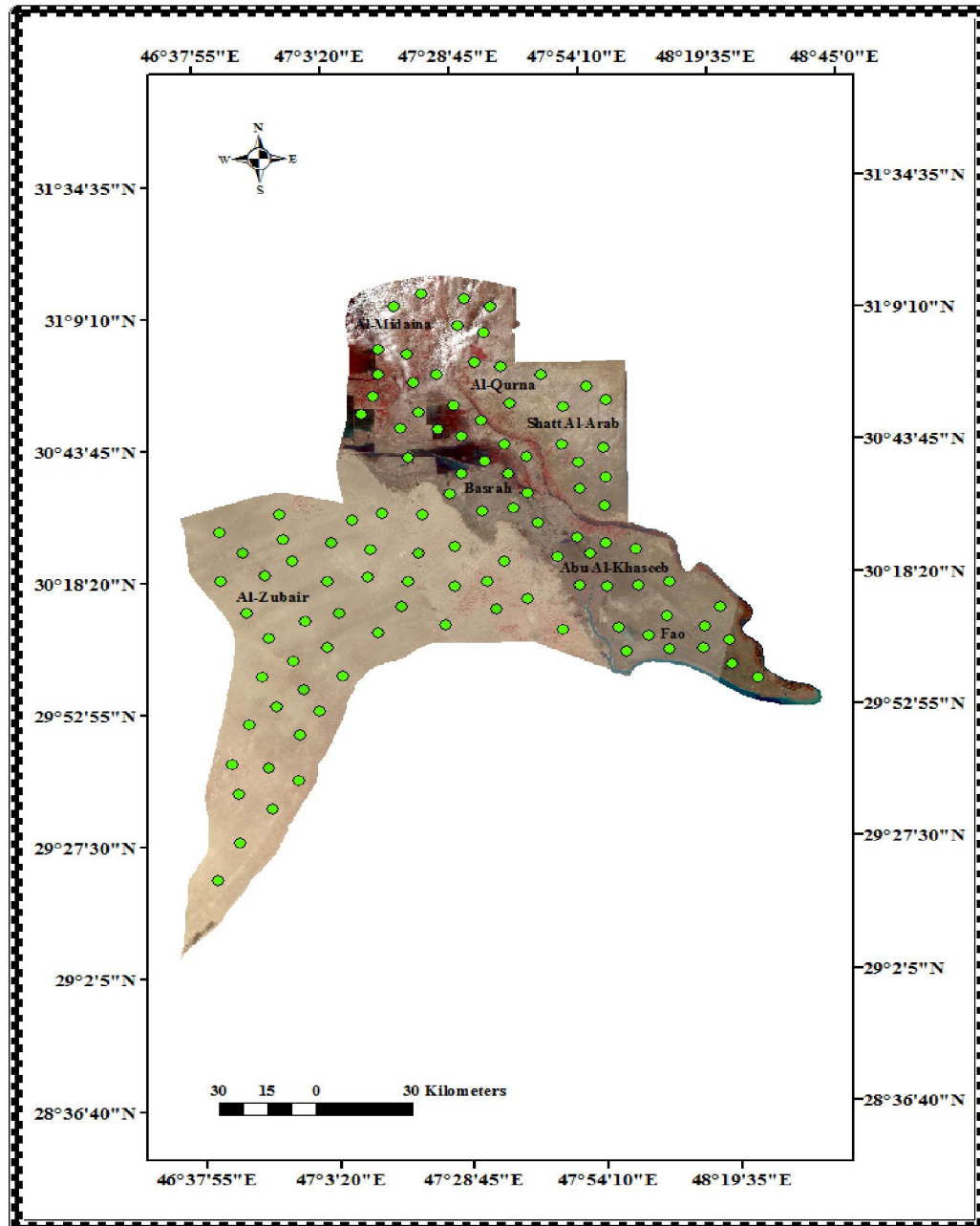
Figure 2. Soil sampling location of the study area.

$$\gamma(h) = C_0 + C\left[\frac{3}{2}\left(\frac{h}{a}\right) - \frac{1}{2}\left(\frac{h}{a}\right)^3\right] \text{ for } 0 < h \le a \ (2)$$
$$\gamma(h) = C_0 + C \text{ for } h > a$$

where C_0 is nugget effect value, C is the partial sill, $(C_0 + C)$ is the sill or total semivariance, a is the range, and h is the distance (Bai et al., 2010).

Cross-semivariances were also calculated to examine a spatial relationship between two variables at the same location. Considering z_u (the primary variable) and z_v (the secondary variable) the variables are said to be co-regionalized or interrelated (Heisel et al., 1999). The cross-semivariance is computed through the equation (3):

$$\gamma_{uv}(h) = \frac{1}{2N(h)}\sum_{i=1}^{N(h)}[z_u(x_i) - z_u(x_i + h)][z_v(x_i) - z_v(x_i + h)] \ (3)$$

where $\gamma_{uv}(h)$ is the cross-semivariance between u and v variables for the interval distance class, h is the lag distance, $N(h)$ is the total number of pairs for lag interval h, $z_u(x_i)$ and $z_u(x_i + h)$ are the measured values of variable z_u, $z_v(x_i)$ and $z_v(x_i + h)$ are the measured values of variable z_v at points x_i and $x_i + h$, respectively. The circular and spherical models provided the best fit for the cross-semivariance for original data of ECe with salinity indices. The circular model defined in the following equation:

$$(h) = C_0 + C\left(1 - \frac{2}{\pi}COS^{-1}\left(\frac{h}{a}\right) + \sqrt{1 - \frac{h^2}{a^2}}\right)$$
$$\text{for } 0 < h \le a \ (4)$$
$$\gamma(h) = C_0 + C \text{ for } h > a$$
$$\gamma(0) = 0$$

To define different classes of spatial dependence for the soil variable, the ratio between the nugget semivariance and the total semivariance or sill was used (Cambardella et al., 1994). If the ratio was ≤ 25%, the variable was considered to be strongly spatially dependent, if the ratio was between 26 and 75%, the soil variable was considered to be moderately spatially dependent; if the ratio was greater than 75%, the soil variable was considered weakly spatially dependent; if the ratio was 100%, or the slope of the semivariogram was close to zero, the

soil variable was considered non-spatially correlated (pure nugget).

Maps of kriged and co-kriged predictions from fitted semivariograms and cross-semivariograms were produced for soil variable using ordinary point kriging interpolation using ArcGIS v.10.4.1 and GS+ v.10 (Gamma Design Software). The accuracy of kriged and co-kriged maps was evaluated using cross validation statistical methods by comparing the actual and predicted values (Santra et al., 2008).

3. Results

The main statistical parameters for ECe data are given in Table (4). ECe values of the study area vary from very strongly saline (>16 dS m^{-1}) to non-saline (0-2 dS m^{-1}) (FAO, 1988). The Coefficient of Variation (CV) of 33.73% confirms that the variability of ECe within the study area was classified as medium (15%-75%) based on the CV values according to the groupings described by Dahiya et al. (1984). The hypothesis that the samples were taken from a random function with a normal distribution was tested using Shapiro–Wilk statistic (Table 5). Correlation analysis between the primary and secondary variables should be as high as possible. Therefore, the Pearson correlation coefficient was applied on the ECe values that were available and remotely sensed data of salinity indices to assess their efficiency in predicting soil salinity using Simple Linear Regression and Multiple Linear Regression techniques (Table 6).

Remotely sensed data with a significant correlation to ECe were considered for developing the regression models. The purpose of this analysis is to select only the salinity index that have high correlation with ECe data. The developed regression models and their statistical results are shown in Table (7). All the developed regression models were highly significant. Among these models, model 1, provided the best fit overall. It had the highest R^2, signifying a strongly linear relationship between BI_1 as an independet variable with ECe value as dependent variable and indicated that 95% of the variance in the ECe values could be explained by this model. However, models 6, 8, and 9 were able to predict soil salinity spatial variation with values of R^2 0.791, 0.837, 0.846 respectively as they met all the model selection criteria.

Table 4. Descriptive statistics of electrical conductivity (ECe).

Soil property	Statistical parameter							
	Mean	Max	Min	Std.Dev.	CV (%)	Median	Skewness	Kurtosis
ECe (dSm^{-1})	61.877	115.000	1.300	20.872	33.732	65.598	-0.203	0.107

Max: maximum; Min: minimum; Std.Dev.: standard deviation; CV: coefficient of variation.

Table 5. Normal distribution test for Electrical Conductivity (ECe).

Variable	W [a]	Normal Dist.	P [b]
ECe dS m^{-1}	0.988	Not rejected	0.478

[a] W = Shapiro–Wilk statistic (Shapiro and Wilk, 1965).

[b] P = significance level; normal distribution is not rejected at P > 0.05.

Table 6. Correlation coefficient between ECe and remotely sensed data.

Soil property	BI_1	BI_2	SI_1	SI_2	SI_3	SI_4	SI_5	SI_6
ECe	0.988[**]	0.875[**]	0.800[**]	0.885[**]	0.891[**]	0.881[**]	0.827[**]	0.852[**]

[**]Correlation is significant at the 0.01 level (2-tailed).

Semivariogram coefficients for original data of ECe with the best-fitted model are listed in Table (8). The R^2 value show that Spherical model fit the experimental semivariogram data very well. The nugget to sill ratio (C_0/C_0+C) expressed as the nugget percentage (Ersahin and Brohi, 2006) was calculated for ECe data and used to evaluate the degree of spatial dependence. The nugget value from resulting experimental semivariogram indicate strong spatial dependence. The range of spatial dependence was about 730.28 m. The range of the semivariogram represents the average distance through which the variable semivariance reaches its peak value.

To assess the accuracy of the Ordinary Kriging geostatistical technique, there is a cross validation analysis for evaluating effective parameters for Kriging. In cross validation analysis a graph can be constructed of the estimated vs. actual values of ECe data for each sample location in the study area. Each point on the graph represents a location in the input data set for which an actual and estimated value are available. The R^2 value is the proportion of variation explained by the best-fit line (Fig. 3).

Cross-semivariograms coefficients of original ECe data with remotely sensed data are shown in Table (9). Cross-semivariograms were calculated to explore and determine spatial interrelations co-regionalized models between ECe and soil salinity indices. Among different experimental cross-semivariogram models tested, Circular, and spherical models were best fitted to the experimental values of ECe with salinity indices. Spatial dependence expressed in percentage (Cambardella et al.,1994). Spatial dependence expressed in percentage (Cambardella et al.,1994). A low ratio (< 25%) means that a large part of the variance is introduced spatially,

implying a strong spatial dependence of the variable. Table (9) shows that all models have relatively low nugget effects suggesting that spatial interrelationships are strong between ECe variable and soil salinity indices considered in this study.

The sampling interval can be determined based on the combination of ECe with BI_1. The cross-variogram between the primary and secondary data sets is modeled (here a low nugget effect) with a fitted range of 468.487m indicating that the intensive sampling scheme used resolved most of the spatial variation. The cross-variogram between ECe and SI_3 data sets shows a Circular model with a fitted range of 299.026m and a low nugget effect indicating a spatial smoothing among adjacent sampling points (Vieira and Gonzalez, 2003). Cross-semivariogram between ECe and SI_5 data sets is modeled with a fitted range of 343.010m, while cross-semivariogram between ECe and SI_6 data sets is modeled with a fitted range of 743.924m indicating that the contribution of the secondary information to the cokriging estimate depended not only on the correlation between primary and secondary variables but also on their patterns of spatial continuity (Goovaerts, 1999).

To assess the accuracy of the Ordinary Cokriging geostatistical technique, there is a cross validation analysis for evaluating effective parameters for Cokriging. In cross-validation analysis a graph can be constructed of the estimated vs. actual values of ECe data for each sample location in the study area (Fig. 4., 5., 6.). The R2 values show that models fit the experimental cross-semivariance data exceptionally well in all cases used in this study. Generally, cross-variograms largely confirmed the findings of the simple correlation analysis, showing more spatial correlation between ECe and remotely sensed data.

Table 7. Developed regression models to predict ECe based on remotely sensed data.

Model	Variable	Constant	Regression Coefficient	Standard Error	R^2
1	BI_1	-10.783	39.617	10.168	0.945**
2	SI_1	-20.573	80.110	12.587	0.640**
3	SI_5	27.344	32.359	11.779	0.684**
4	BI_2 SI_2	-19.332	19.684 42.640	8.957	0.819 **
5	SI_3 SI_4	-19.413	31.231 16.123	8.829	0.824**
6	BI_2 SI_6	0.188	26.271 10.618	9.638	0.791**
7	BI_2 SI_3 SI_4	-19.976	12.956 26.143 9.194	8.582	0.836**
8	SI_2 SI_3 SI_4 SI_5	-33.150	33.422 18.897 20.048 -11.632	8.587	0.837**
9	BI_2 SI_2 SI_3 SI_4 SI_5	-33.537	11.994 27.868 17.240 14.317 -11.772	8.380	0.846**

** Correlation is significant at the 0.01 level (2- tailed).

Table 8. Coefficients of the experimental semivariogram model of Electrical Conductivity (ECe).

Soil property	Model	Nugget, C_0	Sill, $C_0 + C$	Nugget/Sill ratio, C_0/C_0+C %	Spatial dependence level	Range, a (m)	Model R^2	Cross validation R^2
ECe (dS m^{-1})	Spherical	0.005	1.579	0.316	Strong	730.280	0.953	0.458
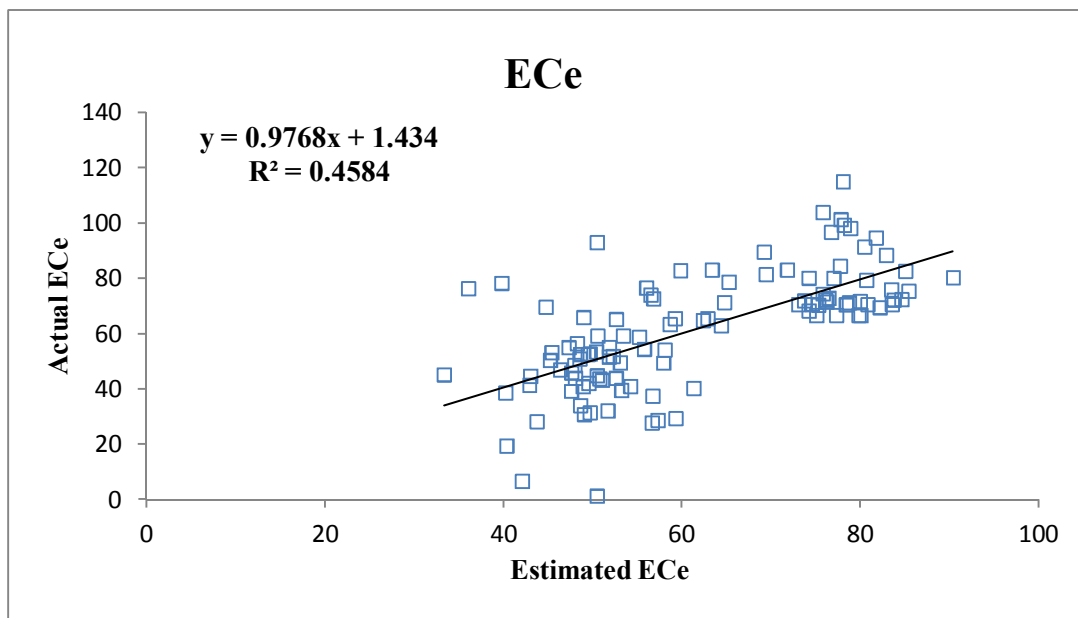
Figure 3. Scatter plots of estimated vs. actual ECe using the experimental semivariogram model.

Table 9. Coefficients of the experimental cross-semivariogram models for combination of Electrical Conductivity (ECe) with remotely sensed data.

Combination of ECe with BI_SI	Model	Nugget, C_0	Sill, $C_0 + C$	Nugget/Sill ratio, C_0/C_0+C %	Spatial dependence level	Range, a (m)	Model R^2	Cross validation R^2
ECe x BI_1	Circular	0.0030	0.362	0.829	Strong	468.487	0.954	0.668
ECe x BI_2	Spherical	0.0044	0.246	1.788	Strong	402.880	0.961	0.619
ECe x SI_1	Circular	0.0004	0.258	0.155	Strong	452.823	0.955	0.557
ECe x SI_2	Circular	0.0003	0.113	0.265	Strong	700.949	0.973	0.613
ECe x SI_3	Circular	0.0040	0.289	1.384	Strong	299.026	0.958	0.633
ECe x SI_4	Circular	0.0025	1.767	0.141	Strong	969.301	0.963	0.610
ECe x SI_5	Circular	0.0024	0.203	1.182	Strong	343.010	0.973	0.601
ECe x SI_6	Circular	0.0033	1.019	0.324	Strong	743.924	0.969	0.610
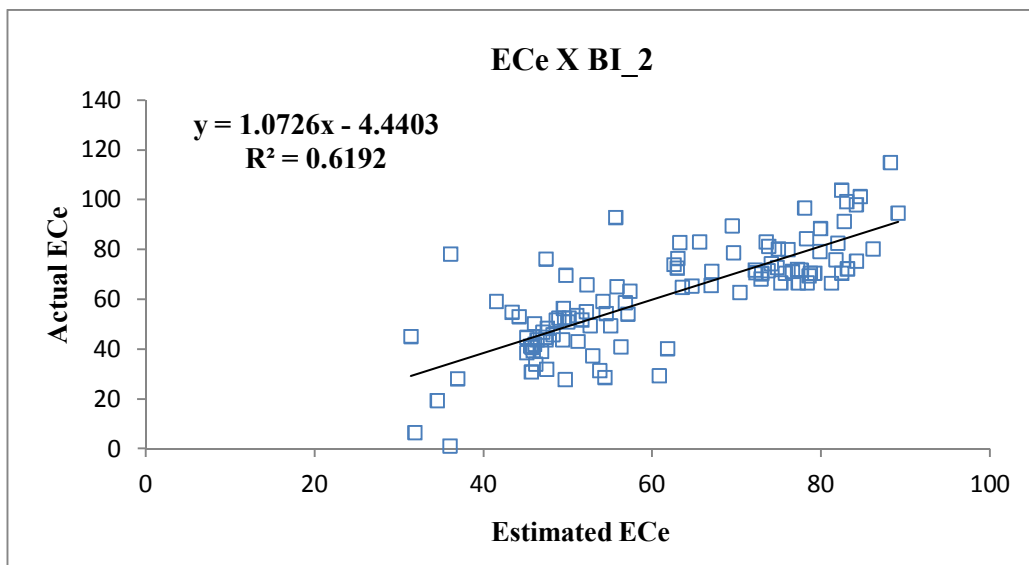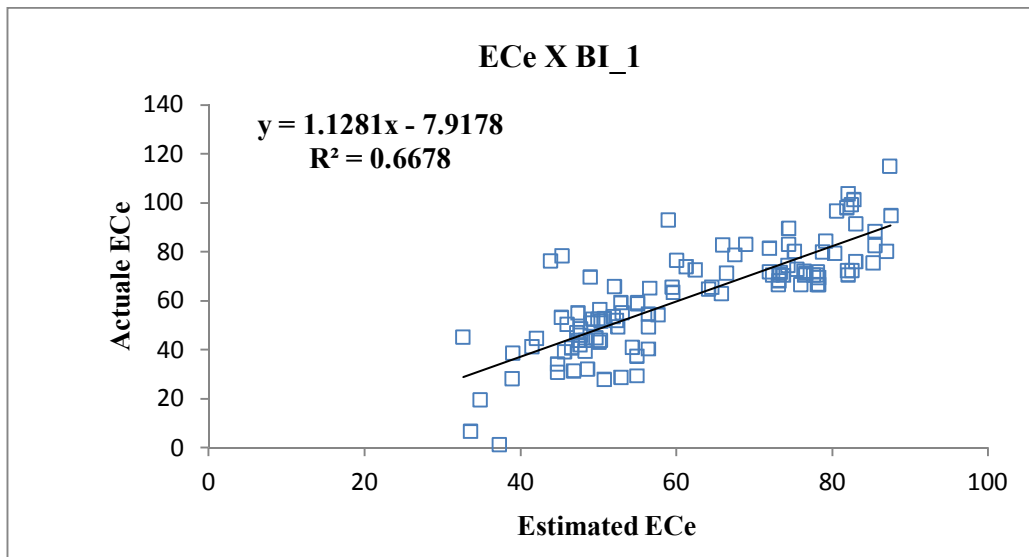
Figure 4. Scatter plots of estimated vs. actual ECe using the experimental cross-semivariogram models for combination of remotely sensed data BI_1, BI_2.
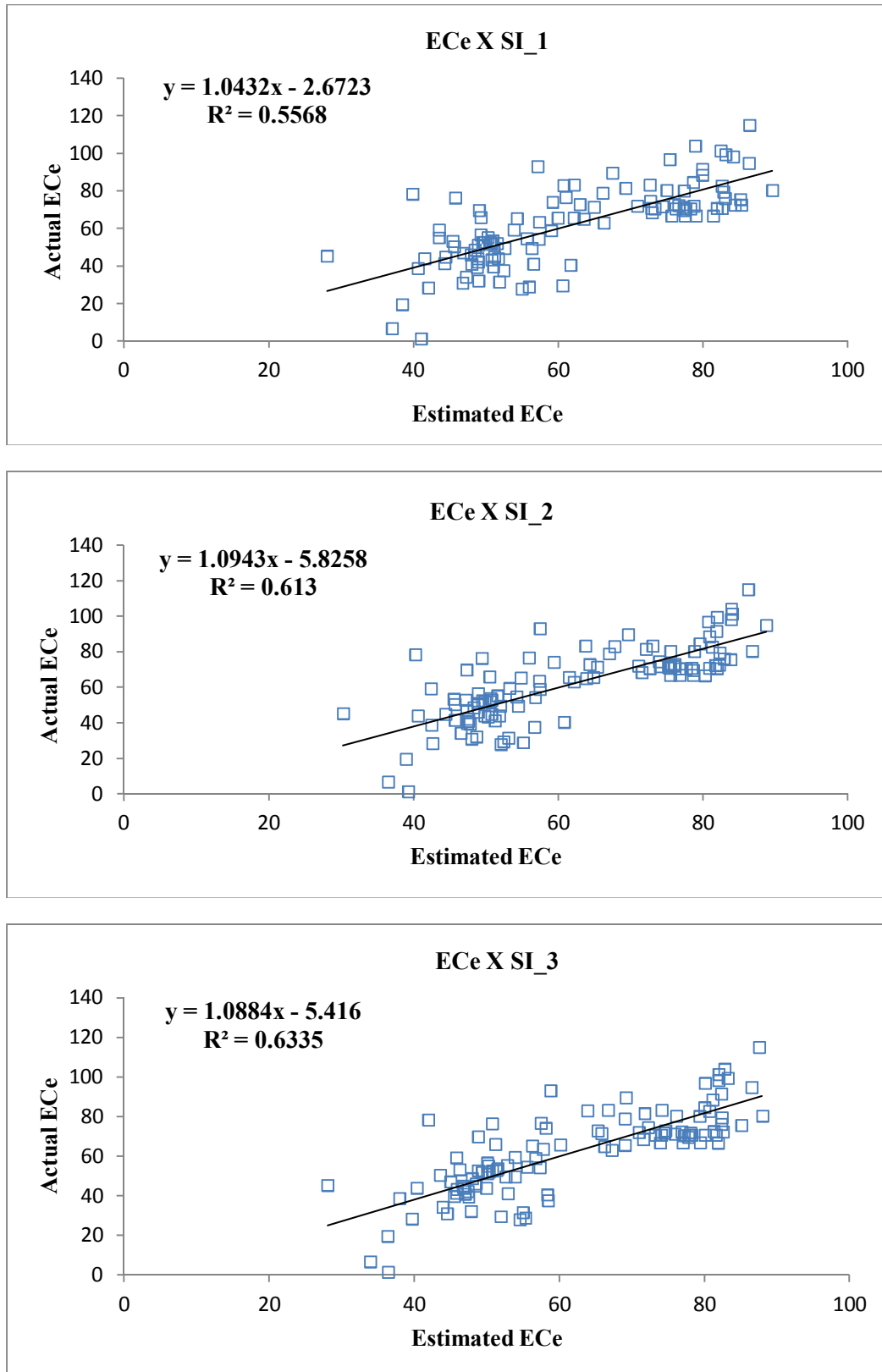
Figure 5. Scatter plots of estimated vs. actual ECe using the experimental cross semivariogram models for combination of remotely sensed data SI_1, SI_2, SI_3.

ECe X SI_4

y = 1.0933x - 5.7144
R² = 0.6105

(Scatter plot: Estimated ECe (x-axis, 0–100) vs Actual ECe (y-axis, 0–140))

ECe X SI_5

y = 1.0798x - 4.8816
R² = 0.6014

(Scatter plot: Estimated ECe (x-axis, 0–100) vs Actual ECe (y-axis, 0–140))

EC X SI_6

y = 1.0844x - 5.2153
R² = 0.6091

(Scatter plot: Estimated ECe (x-axis, 0–100) vs Actual ECe (y-axis, 0–140))
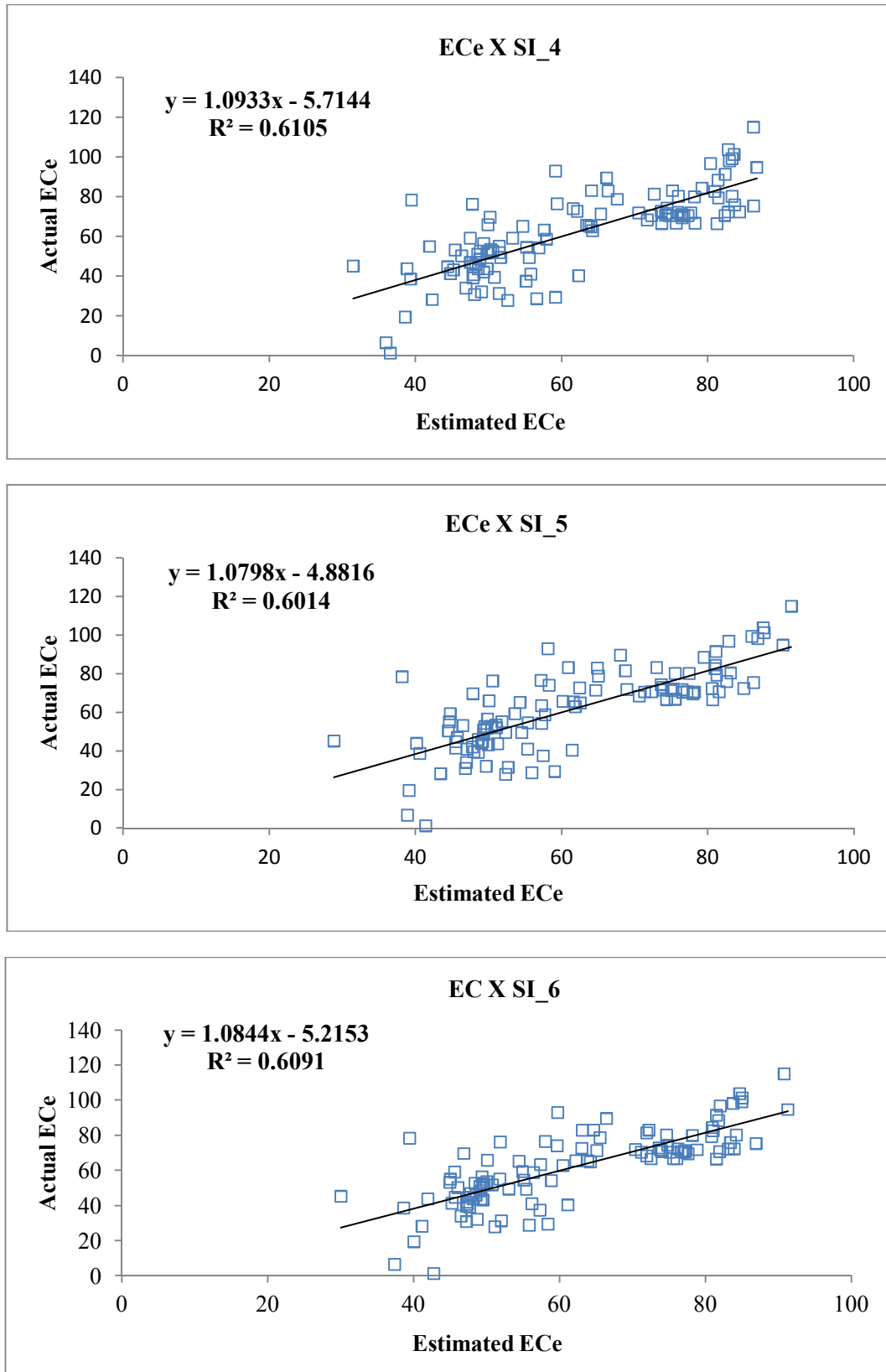
Figure 6. Scatter plots of estimated vs. actual ECe using the experimental cross-semivariogram models for combination of remotely sensed data SI_4, SI_5, SI_6.
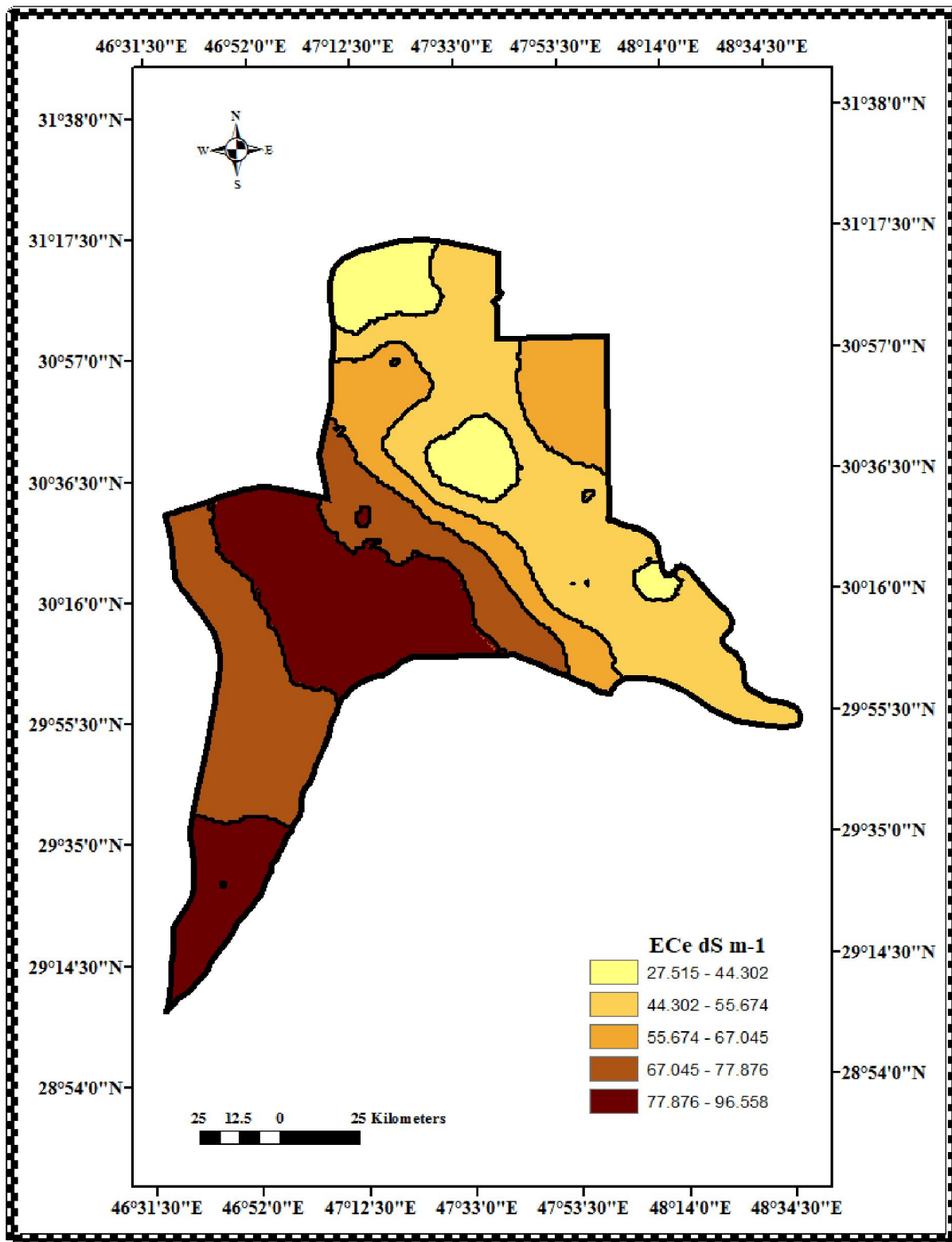
Figure 7. Interpolate- Ordinary Cokriging map of ECe (dS m^{-1})

Spatial prediction map produced by the Ordinary Cokriging procedure using the cross-semivariogram coefficients in Table 9 for the combination of ECe with BI_1 (Fig. 7). The selected model in this study showed superiority in the prediction power ($R^2 = 0.668$) of soil salinity over the study area.

The spatial distribution of ECe showed large surface areas with very strongly saline soil (67.045-96.558 dS m^{-1}) in Al-Zubair and Fao areas follows the pedological variation among desert soils. The spatial patterns of variation in ECe was associated directly to high evaporation, climate, low rainfall history, and local topography.

The spatial prediction map shows also spatial distribution of ECe with lower values (27.515-67.045 dS m^{-1}) in alluvial soils (Al-Midaina, Al-Qurna, Shatt Al-Arab, and Abu Al-Khaseeb areas) compared to desert soils. The lower salinity levels may occur due to farming practices and different irrigation management.

Similarly, spatial distribution of ECe in transition reign between alluvial and desert soils (Basrah) is shown in Fig. (7). The a rising of water table and salt accumulation at the surface combined with a high evaporation rate are one of the most likely factors that have resulted in the spatial variation in soil salinity over this area.

4. Discussion

Factors causing soil salinity include inappropriate and excessive irrigation without an adequate drainage system, irrigation water quality, a rising water table, climate, rainfall history, local topography, and farming practices. This study demonstrates that combining ECe with BI_1 into a regression model offers a potentially quick method to map and model the spatial variation of ECe in the study area. The spatial distribution map drawn based on Ordinary Cokriging explain clearly the spatial variability of the primary variable ECe with the secondary variable BI_1 due to the highest correlation ($R^2 = 0.668$). The method of Ordinary Cokriging significantly improved the accuracy of interpolated Cokriged EC map as compared to Ordinary Kriging.

At the end of the whole procedure, we recommend using independently measured, multivariate secondary information in estimating spatial variability of soil salinity mapping which can be used to implement or support effective soil reclamation programs that minimize or prevent future increases in soil salinity.

Reference

1. Allbed A, Kumar L. Soil salinity mapping and monitoring in arid and semi-arid regions using remote sensing technology: A Review. Advances in Remote Sensing 2013; 2(4): 385-373.

2. Farifteh J, Farshad A, George R J. Assessing salt-affected soils using remote sensing, solute modelling, and geophysics. Geoderma 2006;130(3-4): 206-191.

3. Ghabour T, Daels L. Mapping and monitoring of soil salinity of ISSN. Egyptian Journal of Soil Science 1993;33(4): 370-355.

4. Dale P E R, Hulsman K, Chandica A L. Classification of reflectance on colour infrared aerial photographs and sub-tropical salt-marsh vegetation types. International Journal of Remote Sensing 1986;7(12): 1788-1783.

5. Abbas A, Khan S. Using remote sensing techniques for appraisal of irrigated soil salinity, in Proceedings of the International Congress on Modelling and Simulation (MODSIM'07), L. Oxley and D. Kulasiri, Eds. Modelling and Simulation Society of Australia and NewZealand, Brighton, UK, December 2007: 2638-2632.

6. Al-Marsoumi A M H, Al-Jabbri M H A. Basrah soils; geochemical aspects and physical properties- A Review. Basrah Journal of Science 2007; 25(1): 103- 89.

7. Page A L, Miller R H, Kenncy D R. Method of soil analysis. 1982: Part 2. Agronomy 9.

8. Soil Survey Staff.. Keys to soil taxonomy. 12th (ed.). USDA- Natural Resources Conservation Service 2014:156-107.

9. Khan, N M, Rastoskuev V V, Sato Y, Shiozawa S. Assessment of hydrosaline land degradation by using a simple approach of remote sensing indicators. Agricultural Water Management 2005; 77(1–3): 109- 96.

10. Fourati H T, Bouaziz M, Benzina M, Bouaziz S. Modeling of soil salinity within a semi-arid region using spectral analysis. Arabian Journal of Geosciences 2015;8(12):11182-11175.

11. Khan N M, Rastoskuev V V, Shalina E V, Sato Y. Mapping salt-affected soils using remote sensing indicators-a simple approach with the use of GIS IDRISI. 22nd Asian Conference on Remote Sensing 2001:5-9 November.

12. Douaoui A E K, Nicolas H, Walter C. Detecting salinity hazards within a semiarid context by means of combining soil and remote-sensing data. Geoderma 2006;134(1-2): 230-217.

13. Shapiro S S, Wilk M B. An analysis of variance test for normality (complete samples). Biometrika 1965;52: 611-591.

14. Isaaks H E, Srivastava R M. An introduction to applied geostatistics. University Press, New York, USA. 1989: 561.
15. Bai M, Yinong D X, Pereira L S. Stochastic modeling of basins microtopography: Analysis of spatial variability and model testing. Irrigation Science 2010; 28(2): 172-157.
16. Heisel T, Eraboll A, Andereasen C. Weed mapping with cokriging using soil properties. Precision Agriculture1999;1(1): 52-39.
17. Cambardella C A, Moorman T B, Novak J M, Parkin T B, Karlen D K, Turco R F, A. Konopka E. Field-scale variability of soil properties in central Iowa. Soil Science Society of America Journal 1994; 58(5): 1511-1501.
18. Santra P, Chopra U K, Chakrabory D. Spatial variability of soil properties and its application in predicting surface map of hydraulic parameters in an agricultural farm. Current Science 2008;95(7): 945-937.
19. Food and Agriculture Organization of the United Nations. The salinity and alkalinity status of arid and semi-arid lands. Bull 39, Rome. 1988: 131.
20. Dahiya I S, Richter J, Malik R S. Soil spatial variability: A review. International Journal of Tropical Agricultural 1984;2(1): 102-1.
21. Ersahin S, Brohi A R. Spatial variation of soil water content in topsoil and subsoil of a Typic Ustifluvent. Agricultural Water Management 2006; 83(1): 86-79.
22. Vieira, S R, Gonzalez A P. Analysis of the spatial variability of crop yield and soil properties in small agricultural plots. Bragantia Campina 2003;62(1): 138-127.
23. Goovaerts P. Geostatistics in soil science: state of the-art and perspectives. Geoderma 1999;89: 46-1.

10/18/2017